Supporting information

Self-Shuttle-Mediated Electron Transfer to Boost Photocatalytic Hydrogen Production of Co–Zn Bimetallic MOF

*Taya Ko Saothayanun,[a] Yollada Inchongkol,[a] Nopphon Weeranoppanant,[b] Mio Kondo,[c] Makoto Ogawa [a] and Sareeya Bureekaew *[a]*

[a] School of Energy Science and Engineering (ESE), Vidyasirimedhi Institute of Science and Technology (VISTEC), 555 Moo 1, Payupnai, Wangchan, Rayong 21210, Thailand

[b] Department of Chemical Engineering, Faculty of Engineering, Burapha University, Chonburi 20131, Thailand; School of Biomolecular Science and Engineering (BSE), Vidyasirimedhi Institute of Science and Technology (VISTEC), Rayong 21210, Thailand

[c] Division of Applied Chemistry, Graduate School of Engineering, Osaka University, 2-1 Yamadaoka, Suita, Osaka 565-0871, Japan; Innovative Catalysis Science Division, Institute for Open and Transdisciplinary Research Initiatives (ICS-OTRI), Osaka University, Suita, Osaka 565-0871, Japan; PRESTO, Japan Science and Technology Agency (JST), 4-1-8 Honcho, Kawaguchi, Saitama 332-0012, Japan

**E-mail: sareeya.b@vistec.ac.th*

Experimental sections

Chemicals. Cobalt(II) chloride hexahydrate ($CoCl_2 \cdot 6H_2O$, 98.0%) and Zinc(II) acetate ($Zn(ac)_2$ 99.99%) were purchased from Sigma Aldrich, United states. Zinc(II) chloride ($ZnCl_2$, 95.0%) was purchased from Ajax Finechem, Australia. 1,2,4-triazole (Tz, >99.0%), fluorescein (FI, 98.0%), and triethylamine (TEA, >99.0%) were procured from Tokyo Chemical Industry, Japan. Triethanolamine (TEOA, 99%) was purchased from KemAus, Australia. All chemicals were used as received without further purification.

Preparation of MOFs. A one-pot microwave heating was applied to synthesize $Co_2(tz)_3Cl$, $CoZn(tz)_3Cl$, and $Zn_2(tz)_3Cl$ denoted as Co-tz, CoZn-tz, and Zn-tz, respectively, from aqueous solution of cobalt/zinc precursor (Co:Zn mole ratio of 1:0, 1:1, and 0:1) and 1,2,4-triazole. For Co-tz and CoZn-tz, the solutions of the metal chloride (5.4 mmol) and 1,2,4-triazole ligand (11.6 mmol) were prepared separately by adding the corresponding precursors in 5.0 mL of deionized water each. In the case of Zn-tz, zinc (II) acetate and potassium chloride were used instead of zinc (II) chloride as it led to undesired phase. Then, both solutions were mixed together in a 35 mL microwave vials. The vials were sealed and transferred to a microwave oven (CEM Discovery) and then were heated up to 160^{o}C for 10 min. After cooling down to room temperature, the solid products were collected by centrifugation and washed repeatedly with DI water and methanol. The products were then dried overnight under vacuum at 60^{o}C.

Characterization. Powder X-ray diffraction patterns (XRD) of the products were recorded using Bruker New D8 Advance instrument equipped with Ni filter (Cu Kα radiation). The fresh samples were placed in a PMMA holder for the measurement, while a Si low background holder was used for the sample after photocatalytic testing. Transmission electron microscopy (TEM)

images were obtained using a JEOL JEM-ARM200F high-resolution transmission electron microscopy. Elemental mapping was derived under a scanning transmission electron microscopic (STEM) mode equipped with an energy dispersive X-ray (EDX) analyses using EX-230BU EDX detector. The specimen was prepared by dispersing the products in methanol using ultrasonic homogenizer for a few seconds. Scanning electron micrographs and elemental mapping images were obtained on an Oxford energy dispersive X-ray fluorescence spectrometer (X-Max 150 mm^2) equipped with SEM (JEOL, JSM7610F) instrument. Before SEM measurement, the samples were attached on a carbon tape and coated with Pt by sputtering under vacuum at 10 mA for 20 seconds). UV-Vis diffuse reflectance spectra were recorded on a PerkinElmer Lambda 1050 (PerkinElmer, U.S.A.) using integrated sphere and polytetrafluoroethylene as the reference. Composition of the metals was determined by inductively coupled plasma optical emission spectrometer (ICP-OES) using Agilent Technology 700 Series. The samples were dissolved using 1M HCl solution before ICP measurement. X-ray absorption near edge structure (XANES) analyses of Co K-edge and Zn K-edge were performed at beamline BL1.1W: Multiple X-ray Techniques Beamline, Synchrotron Light Research Institute, Thailand. The measurement was conducted at ambient temperature and pressure by simultaneously measuring the samples together with the Co and Ni foils as standard references for an in-line alignment of the energy shift during the synchrotron-operating time. The data were analyzed using ATHENA software. Thermogravimetric analysis (TGA) was conducted under N_2 atmosphere with the ramping rate of $10^oC\ min^{-1}$ using ThermoPlus EVO2 (Rigaku, Japan). X-Ray Photoelectron Spectroscopy (XPS) was recorded on JEOL JPS-9010MC with a monochromatic Al Kα source (1486.6 eV) at 12 kV and 25 mA under high vacuum (10^{-8} Pa) at room temperature. Prior to the XPS measurement, the powder samples were packed on a carbon tape with area of $9 \times 9\ mm^2$. The obtained spectra

were evaluated using JEOL software to obtain the chemical state of the probing elements and elemental composition. All spectral energies were referenced to the carbon peak C 1s at 284.80 eV.

Stability test. 2.8 ml of TEOA was mixed with 25 ml of DI water to simulate reaction solution during photocatalysis. Afterward, the samples (10 mg) were added into the mixture under vigorous stirring at the controlled temperature (25^{o}C). The mixtures were purged with N_2 gas for 30 min prior to the light irradiation. 300W Xe lamp (TOP-X300, Toption, China) was used as a light source, where visible and UV cut-off filters were equipped to produce UV ($\lambda \leq 405$ nm) and visible light ($\lambda \geq 405$ nm), respectively. The appearance of the suspensions was observed during the light irradiation. The light-exposed products were collected and washed several times using DI water and methanol. XRD and SEM measurement were performed on the dried samples to investigate their stability.

Photocatalytic H_2 evolution reaction. The intrinsic photocatalytic activity of the samples was carried out in the absence of photosensitizer as follows, 2.8 ml of TEOA as sacrificial agent was homogeneously mixed with DI water (25 mL) in the 200-mL photoreactor equipped with quartz window (⌀ 5 cm). For photosensitizer system, the reaction solution was prepared following the abovementioned method except that FI (17 mg) and TEA (3.75 mL) was added as photosensitizer and sacrificial agent, respectively. 10 mg of MOF photocatalysts (Co-tz and CoZn-tz) were added into the mixture. The photoreactor was sealed with septum and degassing by N_2 for 30 minutes. The mixture was irradiated by 300W Xe lamp (TOP-x300, Toption, China) with/without cut-off filters ($\lambda \leq 405$ nm for UV irradiation and $\lambda \geq 405$ nm for visible light irradiation) at controlled temperature (25^{o}C). The evolved gasses in the headspace were collected using 250-µl gas syringe and then were determined by gas chromatography (SHIMAZU GC-

2010 Plus) with a barrier discharge ionization detector (BID) and a SH-Rt 5 Å molecular column (⌀ 0.53 mm x 30 m) using helium as carrier gas.

Photocatalytic test of CoZn-tz was repeated for four cycles under UV-visible light. In each cycle, the collected sample was washed repeatedly with DI water and ethanol to remove the non-adsorbed FI, and then dried overnight. Subsequently, 10 mg of the dried sample was added into water/TEA solution containing the fresh FI under the identical condition.

Apparent quantum efficiency (AQE) of CoZn-tz was assessed under the optimized photocatalytic condition (5 mg catalyst, 25 ml H_2O, 3.75 ml TEA, and 8.5 mg FI) with monochromatic light. A 254 nm LED handheld lamp (6W, Spectroline ENF-260C/FE) and 456 nm LED (12.5W, PR160L, Kessil) were used as the UV and visible light sources, respectively. The power density was recorded to be 1.57 mW cm^{-2} at 254 nm and 24 mW cm^{-2} at 456 nm by illuminometer (pronto-250-plus, Gentec-EO) with the area of 2.8 cm^2. The hydrogen evolved by CoZn-tz was collected after 4 hours of illuminations, so that the AQE was calculated according to the following equation.

$$AQE\ (\%) = \frac{2.4\ \times 10^{8}\ \times R_{H_2}}{I\ \times A\ \times\ \lambda} \times 100\%$$

where R_{H2} is the rate of HER (mol s^{-1}), I is the power density of incident light (W m^{-2}), A is the area of irradiation (m^2), and λ is the wavelength of incident light (nm).

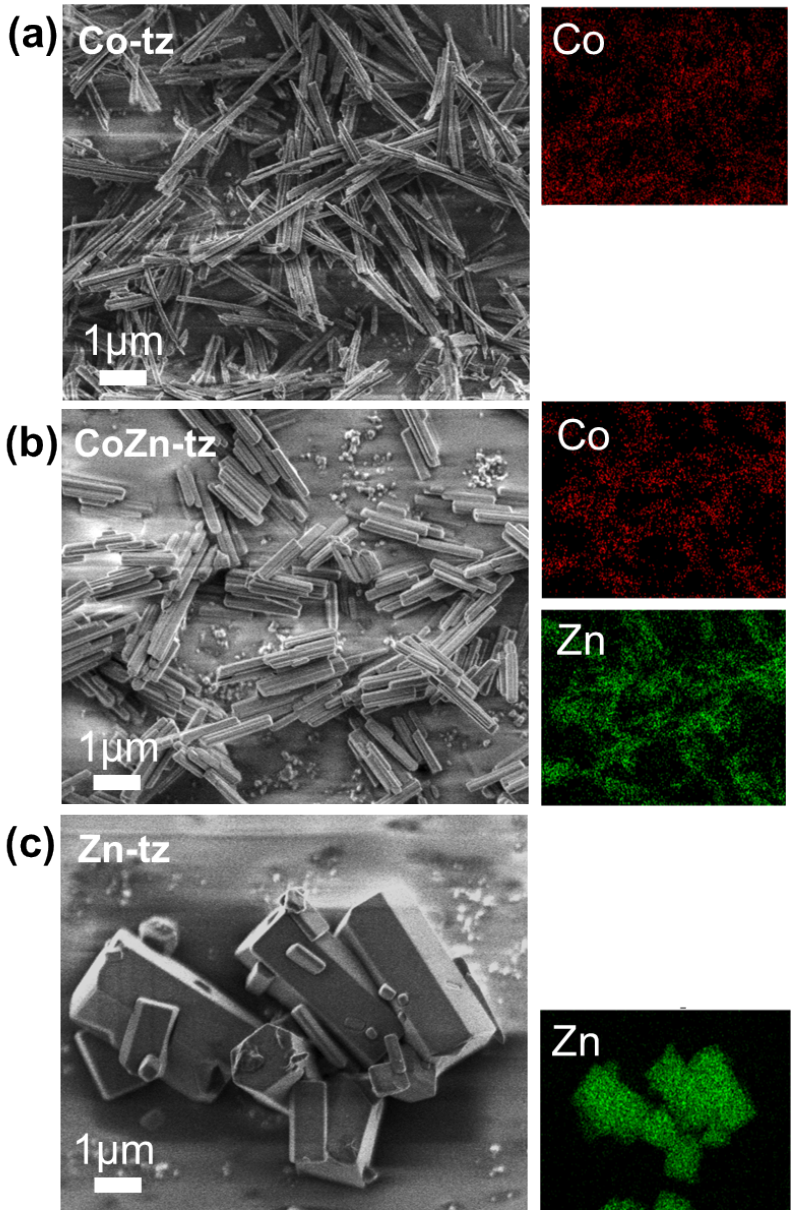

Fig. S1. SEM and EDX images of (a) Co-tz, (b) CoZn-tz, and (c) Zn-tz.

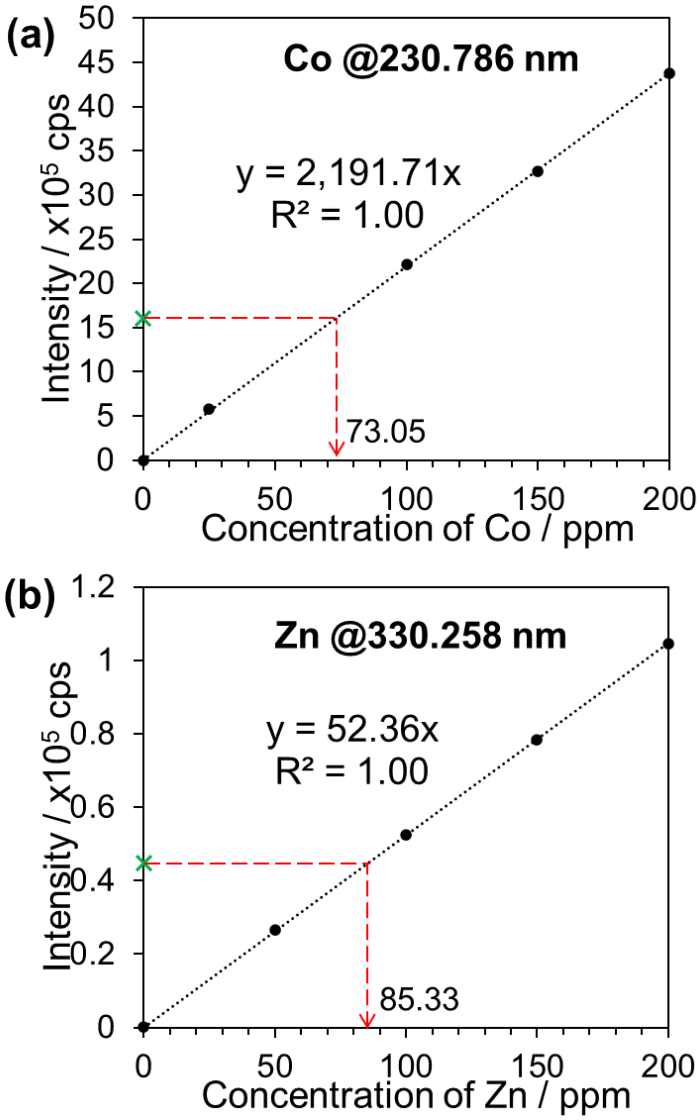

Fig. S2. Calibration curves of (a) Co and (b) Zn by ICP-OES measurement. Prior to the measurement, 4 mg of CoZn-tz are completely digested in 10 ml of 1M HCl and the result are also plotted as green cross-symbol.

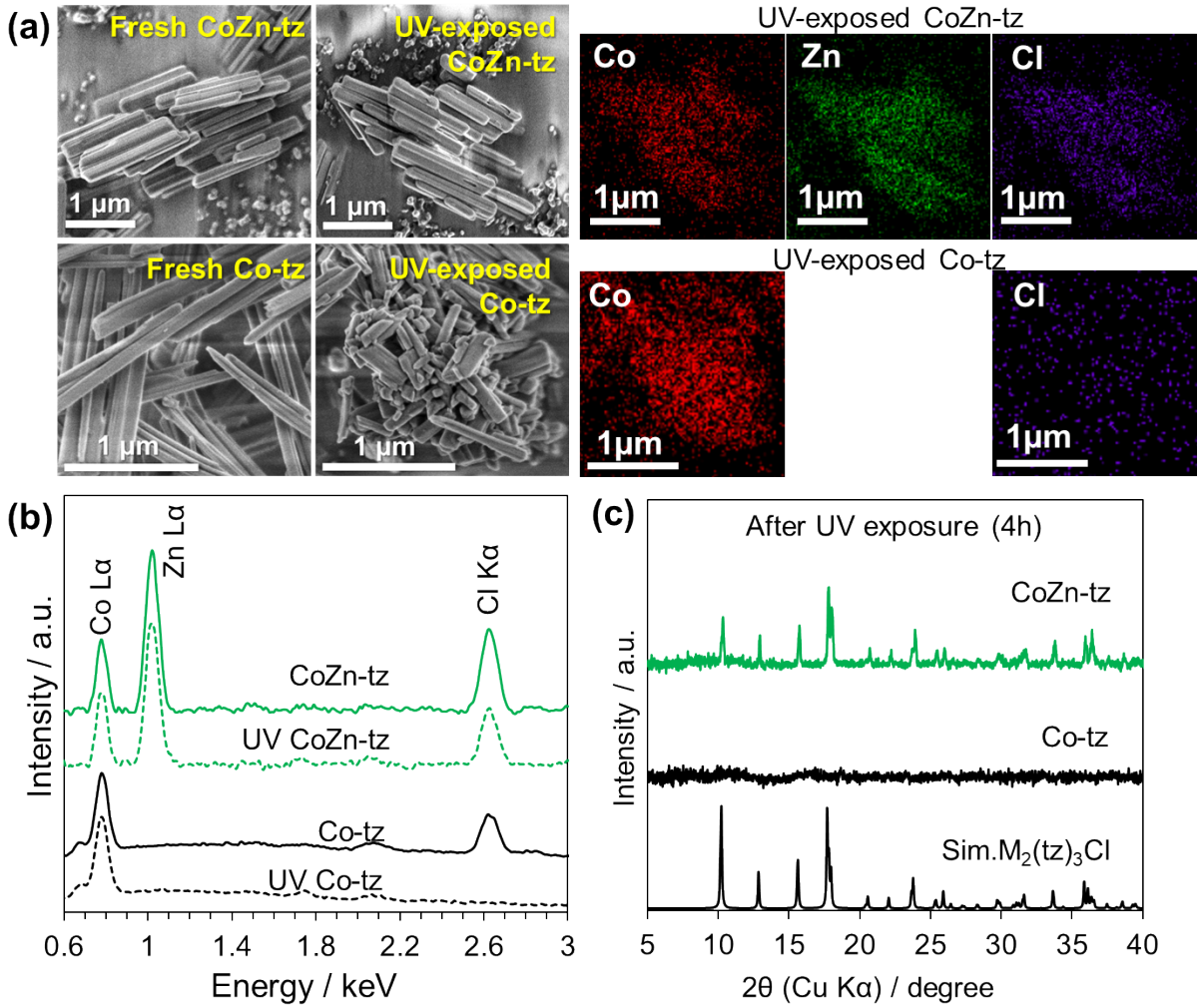

Fig. S3. (a) SEM/EDX images, (b) EDX spectra, and (c) XRD patterns of CoZn-tz and Co-tz before and after exposure to UV (300W Xe, λ≤405 nm) for 4 hours in aqueous TEOA solution.

SEM images of the samples after UV exposure (Fig. S3a) clearly shows cracks in the rod-like particle of Co-tz. In contrast, only small surface scratches are observed in CoZn-tz, plausibly due to particle dispersion and deagglomeration under stirring conditions. Elemental analysis of the UV-exposed samples (Fig. S3a and S3b) revealed no noticeable change compared to the fresh samples, except for a decrease in chloride content in Co-tz for creating active Co_{Td} sites during photocatalysis. XRD patterns (Fig. S3c) of the UV-exposed samples further confirmed that structural integrity of CoZn-tz was preserved.

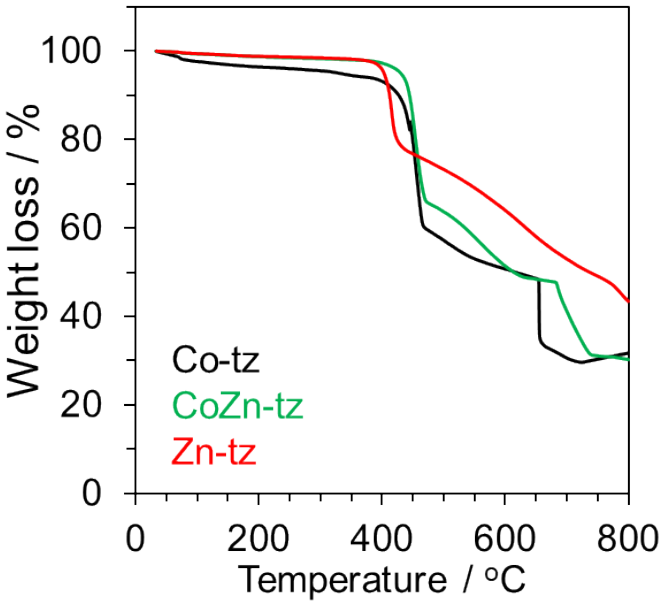

Fig. S4. TGA profiles of the fresh samples.

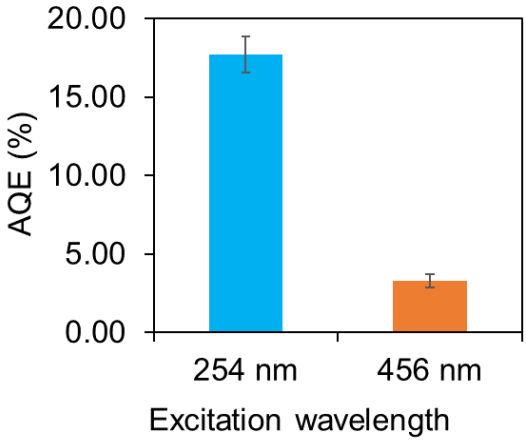

Fig. S5. Apparent quantum efficiency (AQE) of CoZn-tz under excitation of 254 nm and 456 nm. The optimized condition: 5mg catalyst, 25ml H_2O, 3.75 ml TEA, 8.5 mg FI.

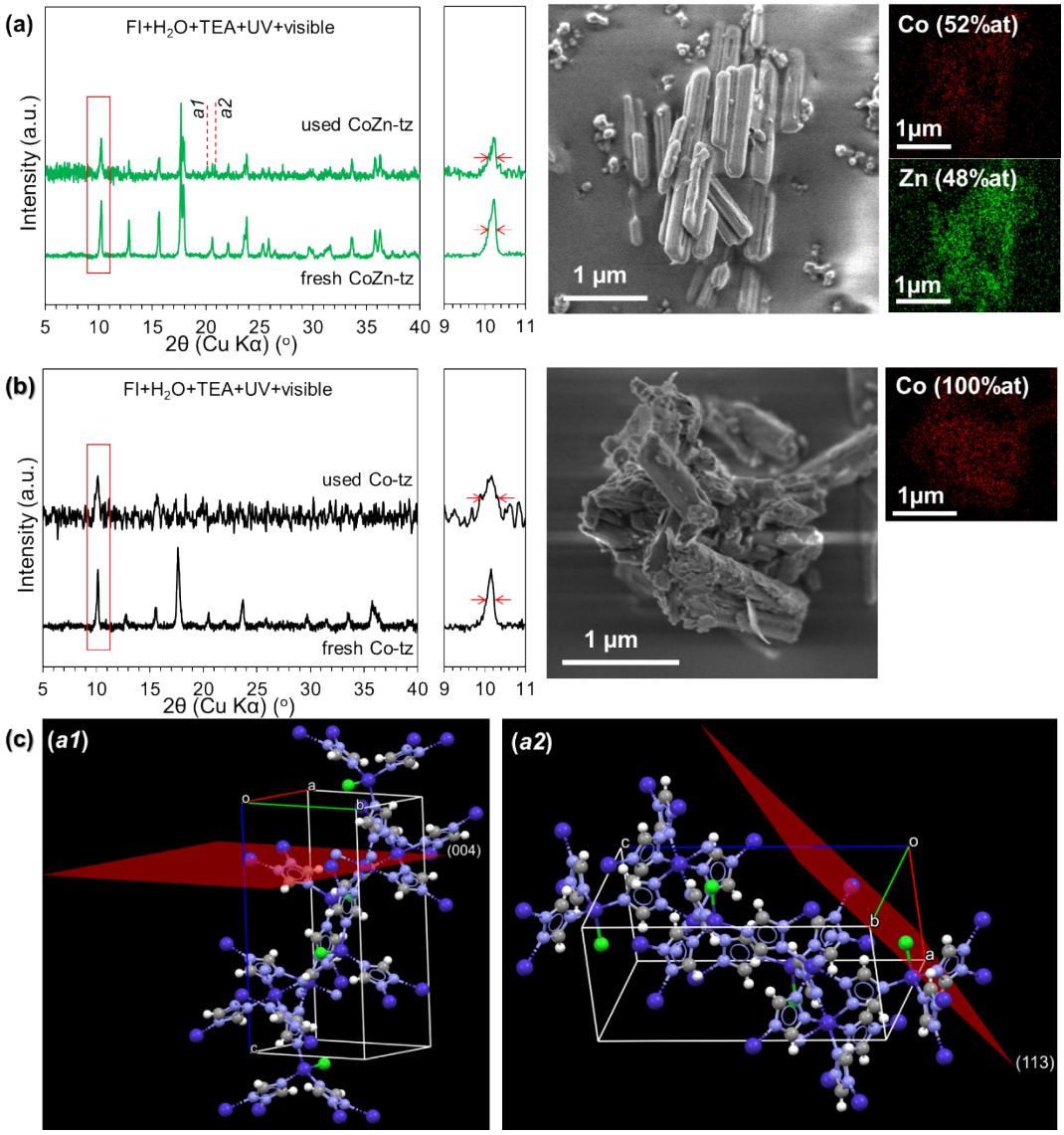

Fig. S6. XRD patterns, the magnified reflections, SEM images, and the corresponding elemental mapping of (a) CoZn-tz and (b) Co-tz after the 1st use under UV-visible light irradiation. The scale bar is 1 μm. (c) Crystallographic images of $M_2(tz)_3Cl$ at *(004)* and *(113)* reflection planes for a1 and a2 as marked in the XRD pattern of the used CoZn-tz.

As shown in Fig. S6a, the main peaks corresponding to $M_2(tz)_3Cl$ are still observed in the XRD pattern of the used CoZn-tz, suggesting the robust structure of CoZn-tz for photocatalytic water splitting. However, some additional reflections around 2θ=20-22° are also appeared as labelled in Fig. S6a (a1 and a1), corresponded to *(004)* and *(113)* planes of the simulated $M_2(tz)_3Cl$ (CCDC 601495). Crystallographic images of the *(004)* and *(113)* planes (Fig. S6c) indicate their projections through tetrahedral Co (Co_{Td}) centers coordinating with chloride anions. This Cl^- can detach upon photocatalytic H_2 evolution reaction to create active sites, altering the coordination environment around the Co_{Td} center. Consequently, the XRD peaks related to these centers change upon the reaction. SEM and EDX analyses of the used CoZn-tz (Fig. S6a) reveal no

noticeable changes of the particle morphology and composition, confirming the preserved structural integrity. In contrast, for the used Co-tz, a broadening of the XRD peak and an absence of some reflections were observed (Fig. S6b), indicating a collapse of the Co-tz structure. This was further confirmed by the SEM and EDX images of the used Co-tz, which showed a rough surface with obvious cracking of particle.

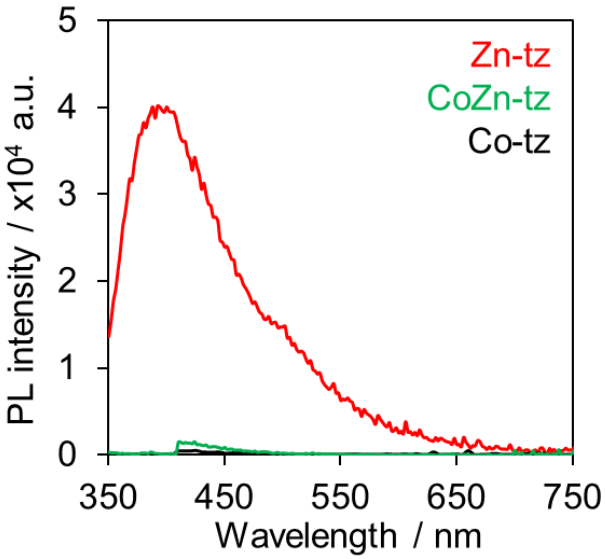

Fig. S7. Steady-state PL spectra of the MOFs at room temperature by an excitation at 330 nm

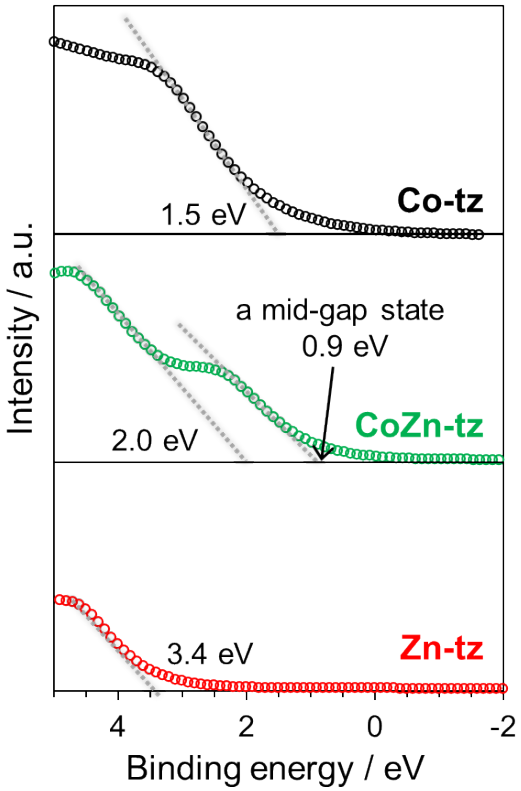

Fig. S8. Valence-band XPS spectra of Co-tz, CoZn-tz, and Zn-tz.

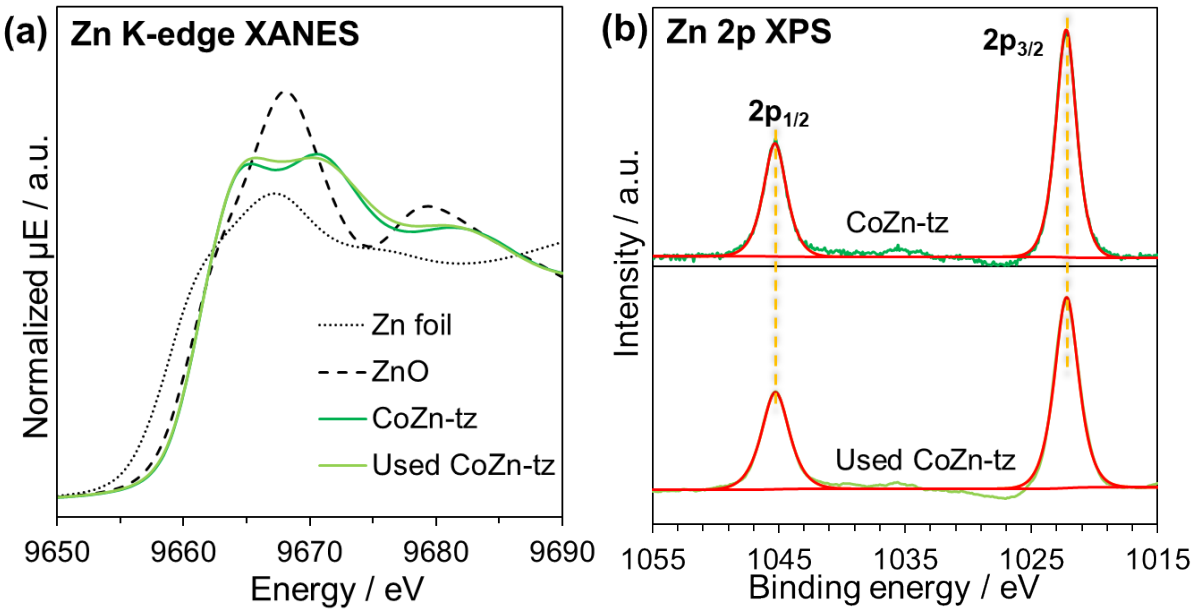

Fig. S9. (a) Zn K-edge XANES and (b) XPS spectra of fresh and 1st used CoZn-tz under UV-visible light irradiation.

Table S1. Absorbance of Co(Td) and Co(Oh) from λ(620 nm) and λ(470 nm)

MOFs	$I_{Co(Td)}$	$I_{Co(Oh)}$	$I_{Co(Td)}/I_{Co(Oh)}$	Co(Td)/Co(Oh)
Co-tz	1.650	0.256	6.45	1[a]
CoZn-tz	0.276	0.257	1.07	0.166[b]
Zn-tz	0	0	-	0

[a] Co-tz contains 50%Co(Td) and 50%Co(Oh).(doi.org/10.1021/ic051992i)

[b] Interpolation from Co-tz and Zn-tz based on Beer-Lambert law.

Calculation of local composition in CoZn-tz

- From Table S2, the following equation can be expressed;

  Co(Td)/Co(Oh) = 0.166 or Co(Td) = 0.166Co(Oh) eq. S1

- Based on ICP-OES and SEM/EDX results, Co content was determined to be 49%;

  Co(Td) + Co(Oh) = 50 eq. S2

- Substituting eq. S1 in eq. S2;

  0.166Co(Oh) + Co(Oh) = 50

  Co(Oh) = 50/1.166 = **43** and **Co(Td) = 7**

- A half of metal occupied in Td and another half in Oh environment;

  Zn(Oh) + Co(Oh) = 50 and Zn(Td) + Co(Td) = 50

  Zn(Oh) = 7 and **Zn(Td) = 43**

Table S2. Comparison of photocatalytic H_2 evolution activity and apparent quantum efficiency (AQE) with various bimetallic MOF photocatalysts.[a]

MOF	Solution	Cocatalyst	Light source	Activity (μmol/g/h)	AQE (%)	Ref
CoZn-tz	FI/H_2O/TEA	-	300W Xe	16,700	17.73 ± 1.16 (@254nm) 3.28 ± 0.42 (@456nm)	This work
Co-tz				5,600	-	
NH_2-UiO-66(Zr/Ti)	H_2O/TEOA	Pt	300W Xe (>420 nm)	389 μmol/mol/h	-	S1
UiO-66(Zr/Ce/Ti)	H_2O	-	Xe (>450 nm)	8.75	0.55 (@300nm)	S2
MIL-173(Zr/Ti)	H_2O	-	150W Hg-Xe (AM1.5G)	17.3	0.11 (@450nm)	S3
PCN-416	MeCN/H_2O/TEOA	Pt	300W Xe (>380 nm)	484	-	S4
NH_2-PCN-415				594	-	
MIL-125(Ti/W)	MeCN/H_2O/TEOA	Pt	300W Xe (>300 nm)	1,110.7	-	S5
MUV-10(Ti/Ca)	H_2O/MeOH	-	300W Xe	125	-	S6
MUV-10(Ti/Mn)				270	-	
ZIF-8(Zn/Cu)	H_2O/Na_2S/Na_2SO_3	-	420W Xe	13,900	9.08 (@420nm)	S7
Ni/Co@NH_2-BDC	MeCN/H_2O/TEA		Solar simulator	150	-	S8
MOF-74(Co/Fe)	$[Ru(bpy)_3]^{2+}$/MeCN/H_2O/TEOA	-	450nm LED	1,214	-	S9
Na/Cu-MOF	FI/EtOH/H_2O/TEA	-	300W Xe	4,650	-	S10
ZZULI-1(Cu/W)	FI/EtOH/H_2O/TEOA	-	300W Xe	6,614	-	S11
PTC-318 (Zr/Co)	MeCN/H_2O/BIH	-	300 W Xe (>420 nm)	16.2	-	S12

[a] Those bimetallic MOF with metalloligand and metal-complex loading were excluded

Table S3. Comparison of photocatalytic H_2 evolution activity and apparent quantum efficiency (AQE) with various monometallic MOF photocatalysts.

MOF	Solution	Cocatalyst	Light source	Activity (μmol/g/h)	AQE (%)	Ref
CoZn-tz	FI/H_2O/TEA	-	300W Xe	16,700	17.73 ± 1.16 (@254nm) 3.28 ± 0.42 (@456nm)	This work
Co-tz				5,600	-	
ZIF-67(Co)	RuN_3/MeCN/H_2O/TEOA	-	405 nm LED	4.85	-	S13
ZIF-67(Co)	$[Ru(bpy)_3]^{2+}$/MeCN/TEOA	-	450 nm LED	1,458	-	S14
Co3-XL	RhB/H_2O/EtOH	Pt	300 W Xe (>320 nm)	23.05	-	S15
LIFM-45	$[Ru(bpy)_3]^{2+}$/DMF/H_2O/TEOA	-	white LED (420-780 nm)	1,102	-	S16
MIL-100(Fe)	H_2O/MeOH	Pt	300W Xe (420-800 nm)	109	-	S17
MIL-53(Fe)	EY/H_2O/TEOA	Pt	300W Xe	700	22.9 (@500nm)	S18
Cu-MOF-1	H_2O/TEOA	-	300W Xe (>420 nm)	1,154	0.034 (@900nm)	S19
Cu-MOF-2				1,398	0.076 (@900nm)	
Cu-RSH MOF	EY/EtOH/H_2O/TEOA	-	300W Xe (>420 nm)	7,880	0.85 (@500nm)	S20
Mixed valence Cu-MOF	H_2O/MeOH	Pt	200W Xe (320-780 nm)	32	2.3 (@420nm)	S21
Cu(II)-MOF	FI/H_2O/TEA	Pt	300W Xe (420-780 nm)	2,510	-	S22

Ni-TBAPy MOF	MeOH/H_2O/ascorbic acid	-	300W Xe (>420 nm)	5,000	8.0 (@420nm)	S23
$Ni_2(PymS)_4$ MOF	FI/H_2O/TEA	-	white LED	6,375	-	S24
IEF-13(Ni)	H_2O/MeOH	-	150W Xe	100	-	S25
			Solar simulator	77.3	-	
	H_2O		150W Xe	7.3	-	
			Solar simulator	2.1	-	
NH_2-MIL-101(Cr)	RhB/H_2O/TEOA	Pt	500W Xe (420-600 nm)	583.3	-	S26
ACM-1	MeCN/H_2O/TEA	Pt	300W Xe (>380 nm)	1675	0.43 (@440nm)	S27
NH_2-MIL-125(Ti)	H_2O/TEOA	Pt (1.5%wt)	500W Xe (>420 nm)	517	2.5 (@365nm)	S28, S29
		Pt (0.5%wt)		367	-	
		-		167	-	
$NH_2/(OH)_2$-MIL-125(Ti)	MeCN/H_2O/TEA	Pt	300W Xe (>420 nm)	707	-	S30
$(SCH_3)_2$-MIL-125(Ti)	H_2O/TEOA	Pt	300W Xe (>400 nm)	3,814	8.9 (@420nm)	S31
NH_2-UiO-66(Zr)	H_2O/MeOH	Pt	200W Hg-Xe	830	3.5 (@370nm)	S32
UiO-66-dcbdt-Cu	$[Ru(bpy)_3]^{2+}$/DMF/H_2O/TEOA	-	white LED (>420 nm)	4,180	-	S33
Co(II)$(bpy)_3$@Zn-PDTP	EtOH/H_2O/TEA	$[Co(bpy)_3]Cl_2$	300 W Xe (>420 nm)	116,800	-	S34
Co-PDTP		-		12,500	-	
Co(II)-Zn-PDTP		-		15,500	-	

References

(S1) Sun, D.; Liu, W.; Qiu, M.; Zhang, Y.; Li, Z. Introduction of a Mediator for Enhancing Photocatalytic Performance via Post-synthetic Metal Exchange in Metal–Organic Frameworks (MOFs). *Chem. Commun.* **2015**, *51*, 2056-2059. (doi.org/10.1039/C4CC09407G)

(S2) Melillo, A.; Cabrero-Antonino, M.; Navalon, S.; Alvaro, M.; Ferrer, B.; Garcia, H. Enhancing visible-light photocatalytic activity for overall water splitting in UiO-66 by controlling metal node composition. *Appl. Catal. B* **2020**, *278*, 119345. (doi.org/10.1016/j.apcatb.2020.119345)

(S3) Gikonyo, B.; Montero-Lanzuela, E.; Baldovi, H.G.; De, S.; Journet, C.; Devic, T.; Guillou, N.; Tiana, D.; Navalon, S.; Fateeya, A. Mixed-Metal Zr/Ti MIL-173 Porphyrinic Metal–Organic Frameworks as Efficient Photocatalysts towards Solar-Driven Overall Water Splitting. *J. Mater. Chem. A* **2022**, *10*, 24938-24950. (doi.org/10.1039/D2TA06652A)

(S4) Yuan,S.; Qin, J.-S.; Xu, H.-Q.; Su, S.; Rossi, D.; Chen, Y.; Zhang, L.; Lollar, C.; Wang, Q.; Jiang, H.-L.; Son, D.H.; Xu, H.; Huang, Z.; Zou, X.; Zhou, H.-C. [$Ti_8Zr_2O_{12}(COO)_{16}$] Cluster: An Ideal Inorganic Building Unit for Photoactive Metal–Organic Frameworks. *ACS Cent. Sci.* **2018**, $_4$, 105–111. (doi.org/10.1021/acscentsci.7b00497)

(S5) Zhang, Y.; Mao, F.; Liu, Y.; Wu, X.; Wen, C.; Dai, S.; Liu, P.; Yang, H. Installation of High-Valence Tungsten in MIL-125(Ti) for Boosted Photocatalytic Hydrogen Evolution. *Sci. China Mater.* **2022**, *65*, 1237-1244. (10.1007/s40843-021-1898-6)

(S6) Castells-Gil, J.; Padial, N.M.; Almora-Barrios, N.; Albero, J.; Ruiz-Salvador, R.; Gonzalez-Platas, J. Garcia, H.; Marti-Gastaldo, C. Chemical Engineering of Photoactivity in Heterometallic Titanium–Organic Frameworks by Metal Doping. *Angew. Chem. Int. Ed.* **2018**, *57*, 8453-8457. (doi.org/10.1002/anie.201802089)

(S7) Varangane, S.; Vennapoosa, C.S.; Tiwari, A.; Nataraj, S.K.; Yendrapati, T.P.; Pal, U. In situ Synthesis of Cu-doped ZIF-8 for Efficient Photocatalytic Water Splitting. *Appl. Organomet. Chem.* **2022**, *36*, e6815. (doi.org/10.1002/aoc.6815)

(S8) Meenu, P.C.; Sha, M.A.; Pavithran, R.; Dilimon, V.S.; Shibli, S.M.A. Stacked Nano Rods of Cobalt and Nickel Based Metal Organic Framework of 2–Amino Benzene Dicarboxylic Acid for Photocatalytic Hydrogen Generation. *Int. J. Hydrog. Energy* **2020**, *45*, 24582-24594. (doi.org/10.1016/j.ijhydene.2020.06.135)

(S9) Zhou, Y.; Hu, W.; Yang, S.; Zhang, Y.; Nyakuchena, J.; Duisenova, K.; Lee, S.; Fan, D.; Huang, J. Site-Selective Probes of Mixed-Node Metal Organic Frameworks for Photocatalytic Hydrogen Generation. *J. Phys. Chem. C* **2020**, *124*, 1405–1412. (doi.org/10.1021/acs.jpcc.9b09634)

(S10) Shi, D.; Cui, C.-J.; Hu, M.; Ren, A.-H.; Song, L.-B.; Liu, C.-S.; Du, M. A Microporous Mixed-Metal (Na/Cu) Mixed-Ligand (Flexible/Rigid) Metal–Organic Framework for

Photocatalytic H_2 Generation. *J. Mater. Chem. C* **2019**, *7*, 10211-10217. (doi.org/10.1039/C9TC03342D)

(S11) Shi, D.; Zheng, R.; Liu, C.-S.; Chen, D.-M.; Zhao, J.; Du, M. Dual-Functionalized Mixed Keggin- and Lindqvist-Type Cu_{24}-Based POM@MOF for Visible-Light-Driven H_2 and O_2 Evolution. *Inorg. Chem*. **2019**, *58*, 7229–7235. (doi.org/10.1021/acs.inorgchem.9b00206)

(S12) Teng, Q.; He, Y.-P.; Chen, S.-M.; Zhang, J. Synthesis of a Zr4(embonate)6–Cobalt Based Superstructure for Photocatalytic Hydrogen Production. *Dalton Trans.* **2022**, *51*, 11612-11616. (doi.org/10.1039/D2DT01976K)

(S13) Yang, S.; Pattengale, B.; Kovrigin, E.L.; Huang, J. Photoactive Zeolitic Imidazolate Framework as Intrinsic Heterogeneous Catalysts for Light-Driven Hydrogen Generation. *ACS Energy Lett*. **2017**, *2*, 75–80. (doi.org/10.1021/acsenergylett.6b00540)

(S14) Pattengale, B.; Yang, S.; Lee, S.; Huang, J. Mechanistic Probes of Zeolitic Imidazolate Framework for Photocatalytic Application. *ACS Catal*. **2017**, *7*, 8446–8453. (doi.org/10.1021/acscatal.7b02467)

(S15) Yang, G.-L.; Che, X.-J.; Hou, S.-L.; Cao, C.-S.; Zhao, B. Photocatalytic Hydrogen Evolution Based on Cobalt–Organic Framework with High Water Vapor Adsorption. *Inorg. Chem*. **2021**, *60*, 1922–1929. (doi.org/10.1021/acs.inorgchem.0c03397)

(S16) Liao, W.-M.; Zhang, J.-H.; Wang, Z.; Lu, Y.-L.; Yin, S.-Y.; Wang, H.-P.; Fan, Y.-N.; Pan, M.; Su, C.-Y. Semiconductive Amine-Functionalized Co(II)-MOF for Visible-Light-Driven Hydrogen Evolution and CO2 Reduction. *Inorg. Chem*. **2018**, *57*, 11436–11442. (doi.org/10.1021/acs.inorgchem.8b01265)

(S17) Wang, D.; Song, Y.; Caim J.; Wu, L.; Li, Z. Effective Photoreduction to Deposit Pt Nanoparticles on MIL-100(Fe) for Visible-Light-Induced Hydrogen Evolution. *New J. Chem.* **2016**, *40*, 9170-9175. (doi.org/10.1039/C6NJ01989G)

(S18) Li, S.; Wu, F.; Lin, R.; Wang, J.; Li, C.; Li, Z.; Jiang, J.; Xiong, Y. Enabling Photocatalytic Hydrogen Production over Fe-based MOFs by Refining Band Structure with Dye Sensitization. *Chem. Eng. J*. **2022**, *429*, 132217. (doi.org/10.1016/j.cej.2021.132217)

(S19) Song, T.; Zhang, L.; Zhang, P.; Zeng, J.; Wang, T.; Ali, A.; Zeng, H. Stable and Improved Visible-Light Photocatalytic Hydrogen Evolution using Copper(ii)–Organic Frameworks: Engineering the Crystal Structures. *J. Mater. Chem. A* **2017**, *5*, 6013-6018. (doi.org/10.1039/C7TA00095B)

(S20) Dong, X.-Y.; Zhang, M.; Pei, R.-B.; Wang, Q.; Wei, D.-H.; Zang, S.-Q.; Fan, Y.-T.; Mak, T.C.W. A Crystalline Copper(II) Coordination Polymer for the Efficient Visible-Light-Driven Generation of Hydrogen. *Angew. Chem. Int. Ed.* **2016**, *55*, 2073-2077. (doi.org/10.1002/anie.201509744)

(S21) Wu, Z.-L.; Wang, C.-H.; Zhao, B.; Dong, J.; Lu, F.; Wang, W.-H.; Wang, W.-C.; Wu, G.-J. A Semi-Conductive Copper–Organic Framework with Two Types of Photocatalytic Activity. *Angew. Chem. Int. Ed.* **2016**, *55*, 4938-4942. (doi.org/10.1002/anie.201508325)

(S22) Li, L.; Zhao, Y.; Wang, Q.; Liu, Z.-Y.; Wang, X.-G.; Yang, E.-C.; Zhao, X.-J. Boosting Photocatalytic Hydrogen Production Activity by a Microporous CuII-MOF Nanoribbon Decorated with Pt Nanoparticles. *Inorg. Chem. Front*. **2021**, *8*, 3556-3565. (doi.org/10.1039/D1QI00516B)

(S23) Liu, L.; Du, S.; Guo, X.; Xiao, Y.; Yin, Z.; Yang, N.; Bao, Y.; Zhu, X.; Jin, S.; Feng, Z.; Zhang, F. Water-Stable Nickel Metal–Organic Framework Nanobelts for Cocatalyst-Free Photocatalytic Water Splitting to Produce Hydrogen. *J. Am. Chem. Soc*. **2022**, *144*, 2747–2754. (doi.org/10.1021/jacs.1c12179)

(S24) Feng, Y.; Chen, C.; Liu, Z.; Fei, B.; Lin, P.; Li, Q.; Sun, S.; Du, S. Application of a Ni Mercaptopyrimidine MOF as Highly Efficient Catalyst for Sunlight-Driven Hydrogen Generation. *J. Mater. Chem. A* **2015**, *3*, 7163-7169. (doi.org/10.1039/C5TA00136F)

(S25) Salcedo-Abraira, P.; Vilela, S.M.F.; Babaryk, A.A.; Cavrero-Antonino, M.; Gregorio, P.; Salles, F.; Navalon, S.; Garcia, H.; Horcajada, P. Nickel Phosphonate MOF as Efficient Water Splitting Photocatalyst. *Nano Res*. **2021**, *14*, 450-457. (doi.org/10.1007/s12274-020-3056-6)

(S26) Wen, M.; Mori, K.; Kamegawa, T.; Yamashita, H. Amine-Functionalized MIL-101(Cr) with Imbedded Platinum Nanoparticles as a Durable Photocatalyst for Hydrogen Production from Water. *Chem. Commun*. **2014**, *50*, 11645-11648. (doi.org/10.1039/C4CC02994A)

(S27) Cadiau, A.; Kolobov, N.; Srinivasan, S.; Goesten, M.G.; Haspel, H.; Bavykina, A.V.; Tchalala, M.R.; Maity, P.; Goryachev, A.; Poryvaev, A.S.; Eddaoudi, M.; Fedin, M.V.; Mohammed, O.F.; Gascon, J. A Titanium Metal–Organic Framework with Visible-Light-Responsive Photocatalytic Activity. *Angew. Chem. Int. Ed*. **2020**, *59*, 13468-13472. (doi.org/10.1002/anie.202000158)

(S28) Horiuchi, Y.; Toyao, T.; Saito, M.; Mochizuki, K.; Iwata, M.; Higashimura, H.; Anpo, M.; Matsuoka, M. Visible-Light-Promoted Photocatalytic Hydrogen Production by Using an Amino-Functionalized Ti(IV) Metal–Organic Framework. *J. Phys. Chem. C* **2012**, *116*, 20848–20853. (doi.org/10.1021/jp3046005)

(S29) Toyao, T.; Saito, M.; Horiuchi, Y.; Mochizuki, K.; Iwata, M.; Higashimura, H.; Matsuoka, M. Efficient Hydrogen Production and Photocatalytic Reduction of Nitrobenzene over a Visible-Light-Responsive Metal–Organic Framework Photocatalyst. *Catal. Sci. Technol*. **2013**, *3*, 2092-2097. (doi.org/10.1039/C3CY00211J)

(S30) Mohammadnezhad, F.; Kampouri, S.; Wolff, S.K.; Xu, Y.; Feyzi, M.; Lee, J.-H.; Ji, X.; Stylianou, K.C. Tuning the Optoelectronic Properties of Hybrid Functionalized MIL-125-NH_2 for Photocatalytic Hydrogen Evolution. *ACS Appl. Mater. Interfaces* **2021**, *13*, 5044–5051. (doi.org/10.1021/acsami.0c19345)

(S31) Han, S.-Y.; Pan, D.-L.; Chen, H.; Bu, X.-B.; Gao, Y.-X.; Gao, H.; Tian, Y.; Li, G.-S.; Wang, G.; Cao, S.-L.; Wan, C.-Q.; Guo, G.-C. A Methylthio-Functionalized-MOF Photocatalyst with High Performance for Visible-Light-Driven H_2 Evolution. *Angew. Chem. Int. Ed*. **2018**, *57*, 9864-9869. (doi.org/10.1002/anie.201806077)

(S32) Silva, C.G.; Luz, I.; Xamena, F.X.L.; Corma, A.; Garcia, H. Water Stable Zr–Benzenedicarboxylate Metal–Organic Frameworks as Photocatalysts for Hydrogen Generation. *Chem. Eur. J*. **2010**, *16*, 11133-11138. (doi.org/10.1002/chem.200903526)

(S33) Zhong, H.; Chen, S.; jiang, Z.; Hu, J.; Dong, J.; Chung, L-H.; Lin, Q.-C.; Ou, W.; Yu, L.; He, J. Utilizing Metal-Thiocatecholate Functionalized UiO-66 Framework for Photocatalytic Hydrogen Evolution Reaction. *Small* **2023**, *19*, 2207266. (doi.org/10.1002/smll.202207266)

(S34) Bai, J.; Wang, J.; Zheng, H.; Zhao, X.; Wu, P.; Pei, L.; Wang, J. Modulating Photoinduced Electron Transfer between Photosensitive MOF and Co(II) Proton Reduction Sites for Boosting Photocatalytic Hydrogen Production. *Small* **2023**, *19*, 2305024. (doi.org/10.1002/smll.202305024)